

Zeolites

One-Pot Synthesis of Zeolitic Strong Solid Bases:
A Family of Alkaline-Earth Metal-Containing Silicalite-1Yu Zhou,^[a] Yanhua Jin,^[a] Meng Wang,^[b] Wei Zhang,^[a] Jingyan Xie,^[a] Jing Gu,^[a]
Haimeng Wen,^[a] Jun Wang,^{*[a]} and Luming Peng^{*[b]}

Abstract: Fabricating stable strong basic sites in well-preserved crystallized zeolitic frameworks still remains a difficult issue. Here, we reported a family of MFI-type metallosilicate zeolites, AeS-1 (Ae: alkaline-earth metal ions of Mg, Ca, Sr or Ba; S-1: silicalite-1) through a direct one-pot hydrothermal method involving the acidic co-hydrolysis/condensation of the silica precursor with the Ae salts. Step-by-step full characterizations were designed and conducted for in-depth discussion of the Ae status in AeS-1. Strong basicity ($H_- \approx 22.5-$

26.5) was detected in AeS-1. The basicity was further confirmed by CO₂ sorption measurements, ¹³C NMR spectra of chloroform-adsorbed samples, and ¹H→¹³C and ¹H→²⁹Si cross-polarization magic-angle spinning NMR spectra of ethyl cyanoacetate-adsorbed samples. The results of Knoevenagel condensations demonstrated the excellent solid base catalysis of AeS-1, which showed high activity, reusability, and shape-selectivity, all of which are explained by Ae-derived zeolitic intracrystalline strong basic sites.

Introduction

Zeolites are a class of well-known environmentally benign catalytic materials with large surface areas and versatile but very stable aluminosilicate crystalline frameworks.^[1–5] In the chemical industry, zeolites have extensive applications as solid acidic catalysts with unique shape-selective properties because of their tunable acidities plus uniform pores.^[6–10] In the past several decades, much research has been devoted to the applications of zeolites in basic catalysis because of their special subnanometer micropores, which provide highly dispersed basic sites and increased selectivity in various reactions.^[8,11–16] The basicity, pore structure, and stability all affect the catalytic performance of basic zeolites,^[8,16–19] as a result, it is a challenge to create highly stable and active strong basic sites in zeolite frameworks while preserving the well-defined intracrystalline channel structures.

Zeolite basicity originates from the negative charge of the framework oxygen atoms.^[13,20,21] The common aluminosilicate zeolite has two primary tetrahedral structural units of SiO₄ and

AlO₄[−], in which the former is neutral whereas the latter usually exhibits acidic properties. Traditionally, basic zeolites can be prepared by ion exchange,^[13,22,23] impregnation,^[24,25] and nitridation.^[12,26] Adding other metal salts during the one-step hydrothermal synthesis of zeolites delivers highly isolated metal ion-related active sites^[27–32] and is also an efficient way to adjust the acid/base properties.^[15,19,33–35] Such synthesis allows the advantages of preserving the zeolitic crystal framework and avoidance of further post-treatment; therefore, it is an energy- and time-saving process. However, previously reported heteroatomic zeolites presented only weak basicity.^[13,20,21] Alkaline-earth (Ae) metals have a low electronegativity of approximately 0.9–1.2, benefiting strong basic sites. For example, magnesia is the most common solid base used in industry.^[11,36] Indeed, Ae ions have been incorporated into aluminophosphates for adjusting acidity,^[37,38] and tetrahedrally coordinated framework magnesium species have been observed in the microporous Mg–Si–O and Al–Si–O materials derived from metal silsesquioxanes.^[39] However, introduction of Ae ions into aluminosilicate or pure silica zeolites through a direct one-pot synthesis has never been reported, except one patent,^[40] which was short of characterization proofs.

Here, we report a family of novel zeolite series, AeS-1 (Ae: alkaline-earth metals of Mg, Ca, Ba, or Sr), in which the alkaline-earth metal ions are incorporated into the widely used MFI-structured pure silica zeolite, silicalite-1 (abbreviated as S-1).^[41] Another reason to choose S-1 (rather than an aluminosilicate zeolite) as the candidate is that this work aims to fabricate strong zeolitic base catalysts and the Al-derived acid sites in aluminosilicate may compromise the created Ae-related basic sites. The synthesis is achieved in a direct one-pot hydrothermal system involving an unconventional acidic pretreatment procedure for co-hydrolysis/condensation of the silica source

[a] Dr. Y. Zhou,[†] Y. Jin,[†] W. Zhang,[†] J. Xie, Dr. J. Gu, Dr. H. Wen, Prof. J. Wang
State Key Laboratory of Materials-Oriented Chemical Engineering
College of Chemistry and Chemical Engineering
Nanjing Tech University (former Nanjing University of Technology)
Nanjing 210009 (P. R. China)
E-mail: junwang@njtech.edu.cn

[b] M. Wang,[†] Dr. L. Peng
Key Laboratory of Mesoscopic Chemistry of MOE
College of Chemistry and Chemical Engineering
Nanjing University, Nanjing 210093 (P. R. China)
E-mail: luming@nju.edu.cn

[†] These authors contributed equally to this work

Supporting information for this article is available on the WWW under
<http://dx.doi.org/10.1002/chem.201501894>.

with Ae salts. Full characterizations are performed on these AeS-1 zeolites, particularly on the typical series MgS-1, including solid-state ^{29}Si and ^{25}Mg NMR spectroscopy. The obtained zeolites present superior strong basicity ($H_- \approx 22.5\text{--}26.5$), and their catalytic performances are tested in the typical base-catalyzed Knoevenagel condensation, demonstrating their high and stable activity as well as the special shape-selectivity.

Table 1. Textural properties and catalytic performance in Knoevenagel condensations.

Sample	Si/Mg ^[a] [mol mol ⁻¹]	Unit cell parameters ^[b]				Surface area [m ² g ⁻¹]	Basic strength [H ₋]
		<i>a</i> [Å]	<i>b</i> [Å]	<i>c</i> [Å]	<i>V</i> [Å ³]		
S-1	∞	19.7208	20.0332	13.0746	5165.39	387	< 15.0
MgS-1(200)	136	19.8554	20.0524	13.1969	5254.32	389	22.5–26.5
MgS-1(100)	125	19.8118	20.0646	13.2404	5263.27	382	22.5–26.5
MgS-1(50)	71	19.9894	20.0971	13.2772	5333.84	380	22.5–26.5
MgS-1(30)	34	20.0358	20.1176	13.3976	5400.20	378	22.5–26.5
MgS-1(20)	25	20.0360	20.1063	13.3597	5381.95	371	22.5–26.5
MgS-1(10)	14	20.0342	20.1100	13.3156	5364.69	367	22.5–26.5
MgO/S-1	35	19.4624	19.9619	12.9194	5019.27	368	15.0–18.4

[a] Si/Mg molar ratios for the final solid products analyzed by ICP. [b] Unit cell volume was determined by using the MDI Jade software (Jade 7 XRD Pattern Processing Software^[42]).

Results and Discussion

MgS-1 zeolites: primary characterizations

Scheme 1 illustrates the synthesis of AeS-1(*n*) (*n* = Si/Ae molar ratio in the initial synthesis gel), where the silica source tetraethylorthosilicate (TEOS) and corresponding Ae (Mg, Ca, Sr, or Ba) ions are co-hydrolyzed and condensed in a moderately acidic environment, followed by basic aging and hydrothermal crystallization. By varying the Mg content in the initial synthesis solution, a series MgS-1(*n*) zeolites are synthesized (Table 1). No crystal structure is obtained when the Mg²⁺ content is too high (*n* ≤ 10). The XRD patterns for calcined MgS-1 display a set of featured peaks indexed to the MFI structure (Figure 1). By contrast, only an amorphous phase is produced under the corresponding basic co-hydrolysis conditions (Figure 1 a), indicating the important role of the unconventional acidic hydrolysis for this synthesis.

Generally, the acidic conditions for hydrolysis and condensation of silica precursors offers a lower reaction rate than a basic one,^[43] allowing more opportunities for isolation and dispersion of metal ions and, thus, promoting the bond formation between metal ions and silanol groups.^[29,33] In this way, it

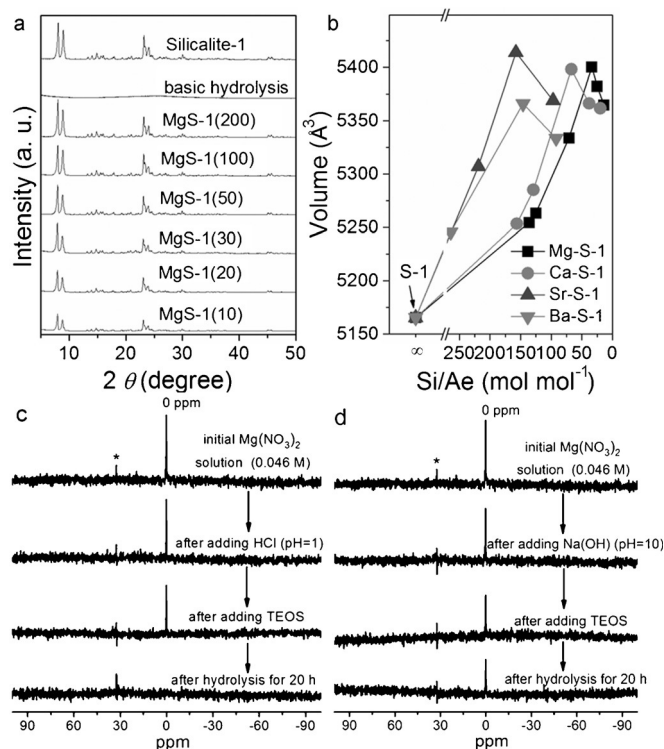


Figure 1. a) XRD patterns for calcined MgS-1. b) Variation of unit-cell volume with Si/Ae molar ratio for all AeS-1 samples. c, d) ^{25}Mg NMR spectra for the solution at different stages during the co-hydrolysis process of the silica and Mg precursors at: c) pH 1, and d) pH 10. Asterisks denote artifacts.



Scheme 1. Schematic diagram of the synthesis procedure for alkaline-earth metal framework-substituted MFI zeolites.

is more likely to generate the desirable Si–O–Ae–O–Si linkage (known as the primary building blocks for further growth of the heteroatomic zeolite crystal) in the gel mixture, ultimately promoting the incorporation of Ae ions into the S-1 framework. To confirm the above speculation, the ^{25}Mg NMR spectrum of the initial synthetic solution (Figure 1 c and d) were measured. The sharp peak at 0 ppm ascribed to the free Mg²⁺ ($\text{Mg}(\text{H}_2\text{O})_6^{2+}$) disappears after hydrolysis at pH 1 for 20 h (Figure 1 c), indicating that the Mg²⁺ is bonded to the silica precursors. Conversely, when hydrolysis occurs at pH 10, significant amounts of free Mg²⁺ can still be detected after 20 h (Figure 1 d), implying that under the conventional basic conditions,

the Mg^{2+} species are unable to link with silanols efficiently to create the primary zeolite-forming units. Moreover, the hydrolyzates of Mg^{2+} under basic conditions can further hamper the crystallization process, generating only an amorphous structure (Figure 1 a). Therefore, the acidic hydrolysis is the key step for successfully obtaining AeS-1 in the present strategy.

The Brunauer–Emmett–Teller (BET) surface areas of these MgS-1 samples are approximately $380 \text{ m}^2 \text{ g}^{-1}$ (Table 1) and similar SEM images are observed compared with the parent sample, S-1 (Figure S1 in the Supporting Information), which features the MFI phase. More notably, the unit-cell volumes expand for all MgS-1 samples, achieving the maximum at $n = 30$ (Table 1 and Figure 1 b), consistent with the larger radius of Mg^{2+} (0.072 nm) over Si^{4+} (0.040 nm). In contrast, no increment of the unit-cell volume is detected for the supported counterpart MgO/S-1. This comparison is indicative of the incorporation of Mg ions into the MFI framework.^[29,33]

The FTIR spectra for MgS-1 (Figure 2 a) all exhibit a new shoulder absorbance band in the wavenumber region of approximately $970\text{--}1000 \text{ cm}^{-1}$, which is absent for S-1 and MgO/S-1. Furthermore, all the MgS-1 products show a broad absorption band at approximately 245 nm in their UV/Vis spectra (Figure 2 b); whereas, this peak is also absent in the control samples of S-1, MgO/S-1, and MgO. In addition, this UV/Vis peak is not seen in the initial gelation stage, however, it emerges and becomes stronger during the crystallization process (Figure S2 in the Supporting Information). This comparison implies the gradual formation of Mg-containing S-1 during the one-pot synthesis, which is different from the simply MgO impregnated counterpart.

The TEM image of MgS-1(30) displays the well-defined uniformly ordered microporous channels and clear electron diffraction pattern of the selected area (Figure 3 a–c), further

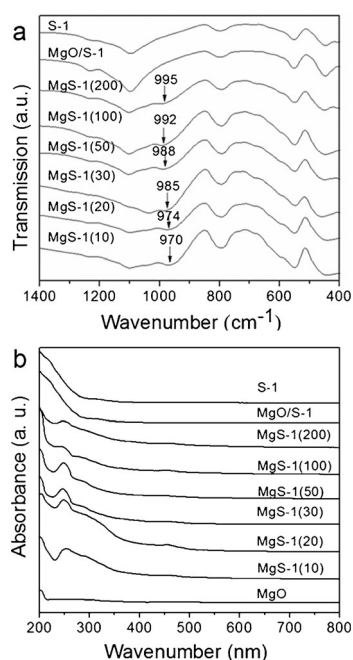


Figure 2. a) FTIR, and b) UV/Vis spectra for MgS-1.

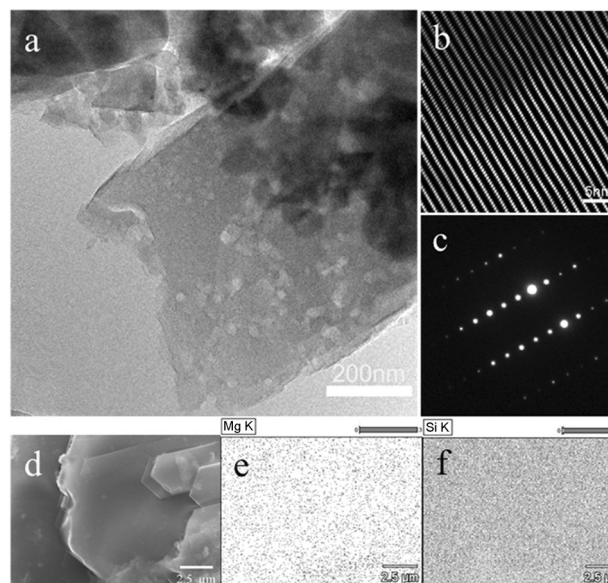


Figure 3. a, b) TEM images of MgS-1(30), and c) the simultaneously recorded small-angle electron diffraction (SAED) pattern from the particle. d) SEM, and e, f) elemental mapping images of Mg and Si on the MgS-1(30) sample.

proving the intrinsic MFI crystal structure as demonstrated by the XRD patterns (Figure 1 a). The inductively coupled plasma mass spectrometry (ICP-MS) analysis confirms the existence of Mg atoms in the solid products (Table 1), and elemental mapping for MgS-1(30) shows that Mg ions distribute uniformly throughout the whole crystal and even in well-crystallized pieces (Figure 3 d–f).

MgS-1 zeolites: further NMR analysis

^{29}Si NMR spectroscopy has been used extensively to illustrate the local structure of zeolites.^[44,45] Figure 4 shows the ^{29}Si magic-angle spinning (MAS) NMR spectra for S-1, the MgS-1 series, and MgO/S-1, as well as the $^1\text{H} \rightarrow ^{29}\text{Si}$ cross-polarization (CP) MAS NMR spectra for MgS-1(30) and MgS-1(10). Fifteen relatively sharp peaks between -108 and -118 ppm (right panel of Figure 4) attributable to Q^4 $[(\text{Si}(\text{OSi})_4)_4]$ sites appears on S-1, reflecting good crystallinity of the highly silicious parent material. The spectral assignment of these peaks to crystallographically inequivalent Si atoms can be found in previous studies.^[46,47] Two additional peaks emerge at -98 and -102 ppm for all the ^{29}Si MAS NMR spectra of the MgS-1 series. With the increase of Mg content, the intensity of the former peaks continuously increases, whereas the latter peaks increase at first, before reaching a maximum for the MgS-1(30) sample, and then decrease (Figure 4). By contrast, the ^{29}Si NMR spectrum for MgO/S-1 is similar to that of S-1, that is, no peak at -98 or -102 ppm is observed. Such comparison suggests that the two signals at -98 and -102 ppm are not assigned to some susceptibility effect caused by extra-framework-doped Mg species and should be attributed to the variation of the internal Si skeletal environment in the presence of Mg salts during the hydrothermal process. Generally, two possible varia-

tions will cause the emergence of more positive Si signals. One is the formation of defectively crystallized zeolitic structures such as terminal Q³ [Si(OSi)₃OH] sites. Secondly, the ²⁹Si chemical shift becomes more positive by introducing other metal ions, for example, trivalent Al ions, into the traditional zeolite framework because of decreased shielding.^[44] To make a clearer identification of the signals at –98 and –102 ppm, the ¹H–²⁹Si CP MAS NMR spectra were measured for all the MgS-1 series as well as S-1 and MgO/S-1 (Figure S3 in the Supporting Information). Selected spectra for the MgS-1(30) and MgS-1(10) samples are presented in Figure 4 to give a comparison with the ²⁹Si MAS NMR spectra. According to the principle of cross polarization, the signal in the ¹H–²⁹Si CP MAS NMR spectrum is attributed to the transfer of magnetization from ¹H to ²⁹Si mediated by the dipolar interaction, which is a through-space rather than through-bond interaction. Here, the CP MAS experiment is utilized to detect the selectively produced signal only from ²⁹Si in close proximity to ¹H nuclei, in other words, no signal can be observed if there is no ¹H existing near the ²⁹Si atoms. As shown in Figure S3 (in the Supporting Information), no signal is observed in the ¹H–²⁹Si CP MAS NMR spectra of S-1 and MgO/S-1, in accordance with the well-crystallized structure of these two samples (all the silica exists in the form of Q⁴ [(Si(OSi)₄] as demonstrated by the ²⁹Si MAS NMR spectra), which provides no possible ¹H atoms near the ²⁹Si to produce the CP signal. A single peak at –98 ppm is observed in each MgS-1 sample and this can be attributed to terminal Q³ [Si(O-Si)₃OH] groups (Figures 4 and Figure S3 in the Supporting Information). The intensity of this peak increases with more Mg ions, consistent with the presence of more cracks on the crystal surface. No resonance at –102 ppm is detected in the ¹H–²⁹Si CP MAS NMR spectra of any of the MgS-1 samples, suggesting that the signals at –102 ppm in the ²⁹Si MAS NMR spectra of the MgS-1 series do not arise from the defectively crystallized zeolite structure. Therefore, this signal is tentatively assigned to the contribution of the framework Mg species.^[43] Moreover, with the increase of the Mg content, two variations can be observed in the ²⁹Si MAS NMR spectra of the MgS-1 series: 1) the peak intensity at –102 ppm increases at low Mg content, reaching the highest value for MgS-1(30), and then decreases; 2) the line widths of the Q⁴ resonances (right panel of Figure 4) first become significantly broader with increasing Mg content, then slightly narrower. The above variations are in accordance with the enlargement of the unit-cell volumes (Figure 1 b), and are also in agreement with the existence of framework Mg ions at the lower Mg contents and the emergence of extra-framework magnesia at higher Mg loadings.^[45]

²⁵Mg MAS NMR spectroscopy was employed for more insight into the state of the Mg species in MgS-1(30). ²⁵Mg isotopically labeled precursor was used to prepare a ²⁵Mg isotope enriched ²⁵MgS-1(30) sample to enhance the NMR signal. Nevertheless, no signal was observable, implying the large quadrupolar coupling constants of Mg ions in the Mg-incorporated distorted framework environment. Therefore, we designed a successive process, in which the ²⁵MgS-1(30) sample is calcined, followed with water adsorption, and then water removal through calcination, to monitor the variation of ²⁵Mg signal in

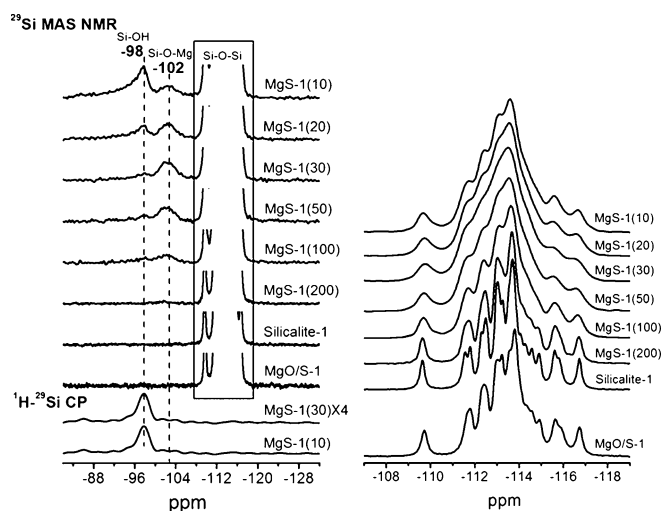


Figure 4. ²⁹Si MAS NMR spectra for S-1, the MgS-1(*n*) series, and MgO/S-1 in comparison to ¹H→²⁹Si CP MAS NMR spectra for the MgS-1(*n*) series. The ²⁹Si MAS NMR spectra in the frequency of –107 to –119 ppm are zoomed in on the right.

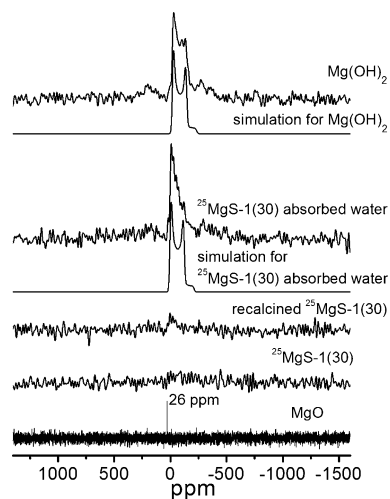


Figure 5. ²⁵Mg MAS NMR spectra for ²⁵MgO and ²⁵MgS-1(30) treated successively by in situ calcination, water adsorption, and finally water removal through calcination, as well as Mg(OH)₂ for reference. Line shape simulations for Mg(OH)₂ (iso = 13.5, CQ = 3.15 MHz, Q = 0.0) and ²⁵MgS-1(30) adsorbed with water (iso = 35, CQ = 3.15 MHz, Q = 0.0) are shown for comparison.

each step. The designing of above experiment was inspired by the early ²⁷Al NMR studies of aluminosilicate zeolites,^[48,49] which reported that the framework Al species changed from tetrahedral to octahedral by adsorbing water and reversed back to tetrahedral by desorbing the water, while the extra-framework Al species gave no such variation. Therefore, the purpose of our experiment is to detect the possible variation of the Mg species in MgS-1(30) sample by water adsorption. As shown in Figure 5, although no signal appears for the calcined ²⁵MgS-1(30) sample, a wide signal ranging from approximately 30 to –230 ppm is detected after it is exposed to moisture. The simulated spectrum verifies that this peak is associated with a similar quadrupolar coupling constant (CQ) and asym-

metry parameter (Q) to the octahedrally coordinated Mg species in $\text{Mg}(\text{OH})_2$. However, the different isotropic (iso) chemical shift excludes the possible formation of nano-sized $\text{Mg}(\text{OH})_2$ during the water adsorption process. Therefore, the signal of the water-adsorbed $^{25}\text{MgS-1(30)}$ can be interpreted as follows: water adsorption has relaxed the much-distorted framework Mg-containing structure (with mostly tetrahedral Mg species) into octahedrally coordinated Mg species through the binding of two H_2O molecules, leading to a much smaller quadrupolar coupling constant and the appearance of a ^{25}Mg signal. The peak disappears again after water removal, indicating that the Mg species may return back to the distorted framework structure. The phenomenon also implies that the formed framework Mg species are stable in contact with water.

Base properties

The basicity of the obtained MgS-1 was investigated by the Hammett indicator method, carbon dioxide sorption, and ^{13}C MAS NMR analysis of $^{13}\text{CHCl}_3$ adsorbed over zeolites. The Hammett indicator method shows that the MgS-1 series all present strong basicity with H_- in the range of approximately 22.5–26.5, much higher than S-1 itself ($H_- < 15.0$) or the impregnated counterpart MgO/S-1 ($H_- \approx 15.0$ –18.4; Table 1), indicating that the strong basicity has been generated through our one-pot hydrothermal synthesis. The ^{13}C MAS NMR spectra of $^{13}\text{CHCl}_3$ adsorbed over MgO/S-1, S-1, and MgS-1(30) (Figure 6a) indicate that MgO/S-1 shows the same chemical shift as S-1 whereas a signal centred at a higher frequency is observed for MgS-1(30), further indicating the enhanced basic strength of MgS-1.^[50] The CO_2 adsorption of MgS-1, S-1, and MgO/S-1 were assessed at 100°C . No CO_2 uptake was detected in the adsorption–desorption isotherms of the S-1 and MgO/S-1 samples, suggesting that CO_2 molecules are hardly adsorbed on these two weakly basic samples under these conditions.

By contrast, MgS-1(30) exhibits apparent CO_2 uptake of about 21 mg g^{-1} (0.477 mmol g^{-1} ; Figure 6b), indicating that incorporating Mg^{2+} into the S-1 framework can significantly improve the basicity of zeolite, allowing the capture of CO_2 at high temperature. It is rational to expect this zeolitic frame-

work Mg^{2+} -derived strong base to be potentially very important for catalytic applications.^[30,51]

CaS-1, SrS-1, and BaS-1 zeolites

Parallel to MgS-1 and following the same acidic co-hydrolysis synthetic route shown in Scheme 1, we also synthesized and characterized three other Ae containing S-1 species (CaS-1, SrS-1, and BaS-1). Highly crystallized Ca-, Sr-, and Ba-containing S-1 can be prepared and show similar structure variation to MgS-1; for example, the expanding of the unit-cell volume and the new peaks in the IR and UV/Vis spectra (Table S1, Figures S4 and S5 in the Supporting Information). In addition, all of these samples show the strongly basic strength of $H_- \approx 22.5$ –26.5. However, compared with the radius of Mg^{2+} (0.072 nm), the much larger radii of Ca^{2+} (0.099 nm), Sr^{2+} (0.112 nm), and Ba^{2+} (0.135 nm) make them more difficult to be incorporated into the zeolite framework; as a result, their synthetic windows are narrower than that of MgS-1. Actually, Ca (Sr, Ba)S-1 crystals can only be obtained with lower Ae contents ($n \leq 20$ for CaS-1, and $n \leq 50$ for SrS-1 or BaS-1) with the most expanded unit-cell volume being detected at $n = 100$ for Ca, Sr, and Ba-containing samples (Figure S3b–d in the Supporting Information).

Catalytic studies

The catalytic activities of the AeS-1 series were tested in the Knoevenagel condensation of benzaldehyde and ethyl cyanoacetate (Scheme S1 in the Supporting Information), which is a probe reaction typically used for evaluating basic catalysts.^[52] The target product, ethyl-2-cyano-3-phenyl acrylate, is detected exclusively with the tested catalysts. As shown in Figure 7, the conversion of ethyl cyanoacetate over pure S-1 (30.6%) is only slightly higher than the non-catalytic system (24.7%), whereas AeS-1 catalysts exhibit dramatically enhanced activities (Figure 7 and Table S1 in the Supporting Information). Over MgS-1(30), CaS-1(100), SrS-1(100), and BaS-1(100), the conversions reach their respective maximum values of 95.2, 96.2, 91.9, and 91.6%, all of which are about twice those over the supported counterparts, AeO/S-1. The conversion by MgS-1(30) even exceeds the traditionally strong solid base of pure MgO (93%, Figure 7). Furthermore, in term of TOF (turnover frequency), MgS-1(30) (40 h^{-1} , Figure 7) is much more active than MgO (0.74 h^{-1} , Figure 7); this is probably due to the non-porosity of the latter. A five-run catalytic recycling test was applied to investigate the reusability of selected AeS-1 samples and good reusability is observed with MgS-1(30) and CaS-1(100) (Table S2 in the Supporting Information).

For further comparison, pure ZSM-5 and Fe-containing heteroatomic ZSM-5 zeolite, FeZSM-5(100), were prepared according to ref. [33] (the corresponding textural properties are in Table S3 in the Supporting Information) and their catalytic performances were assessed under the same conditions. The classical ZSM-5, with aluminum metal ions and is often used as a solid acid catalyst, shows an inferior conversion of 34.9% (Figure 7). In previous work, FeZSM-5(100) showed good activity in catalyzing the Knoevenagel condensation of benzalde-

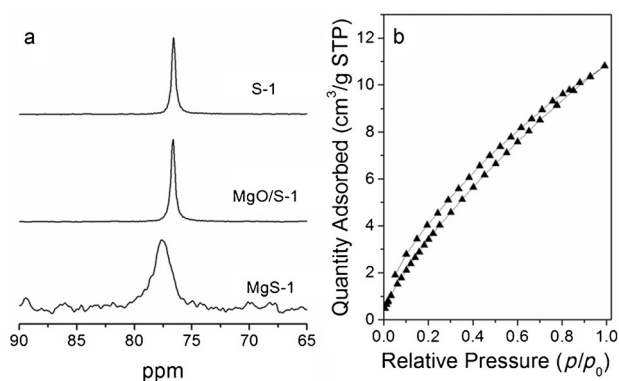


Figure 6. a) ^{13}C MAS NMR spectra of $^{13}\text{CHCl}_3$ adsorbed over S-1, MgO/S-1, and MgS-1(30); b) CO_2 sorption isotherm of MgS-1(30) at 373 K.

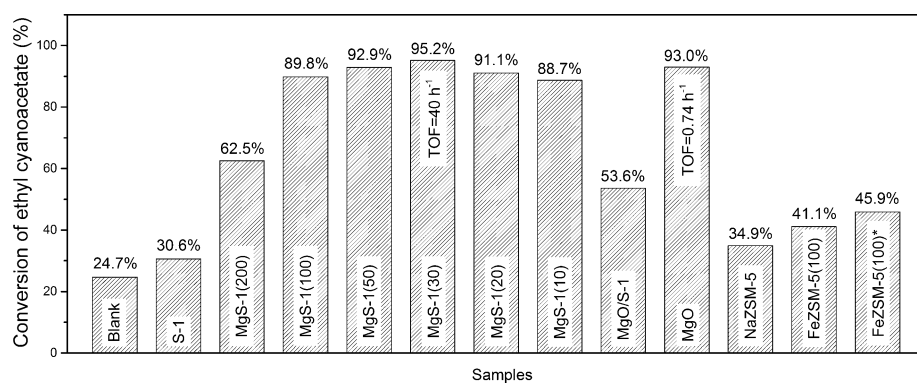


Figure 7. Knoevenagel condensation of benzaldehyde with ethyl cyanoacetate over various catalysts. Reaction conditions: catalyst 0.1 g, benzaldehyde 8 mmol, ethyl cyanoacetate 8 mmol, ethanol 5 mL, 70 °C, 4 h. *: reaction time: 12 h, reaction temperature: 90 °C.

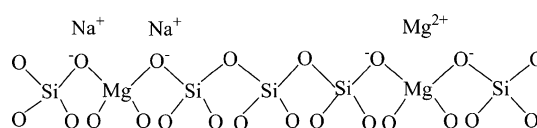
hyde with malononitrile,^[33] however, if more inert ethyl cyanoacetate^[53,54] instead of malononitrile is used as the substrate, the conversion drops to 41.1%. It still gives a low conversion of 45.9% even when the reaction temperature is raised from 70 to 90 °C and at the much elongated time of 12 h (Figure 7), indicating that Fe ions in the MFI framework cannot provide suitable basicity for efficiently catalyzing the Knoevenagel condensation of benzaldehyde and ethyl cyanoacetate. All the comparison results strongly demonstrate the much better activity of the AeS-1 zeolites, which is most probably associated with the well-isolated framework Ae²⁺-derived strongly basic sites.

It is also interesting to note that these AeS-1 catalysts can be similarly active after full exposure to air without any in situ activation, that is, the strongly solid basic sites are capable of resisting possible contamination by water and CO₂ in air (Table S2 in the Supporting Information). Moreover, strong and stable basic sites within the well-defined zeolitic intracrystalline micropores allow us to expect a possible shape-selective effect in the base-catalyzed reaction. Indeed, by comparing catalytic performances of MgS-1 and pure MgO in Knoevenagel condensations with varied substrates (Table S4 in the Supporting Information), it can be found that the activity of the former is sensitive to the molecular size of the substrates, whereas the latter is not, revealing the significant influence of the uniform micropores and implying a reactant-controlled shape-selectivity effect on the catalytic process.

Based on the above results, we tentatively propose basic sites in AeS-1 samples (Scheme 2). Taking MgS-1(30) as an example, ion exchange tests show that the obtained AeS-1 samples are capable of ion exchange, and the counter cations are Na⁺ and Mg²⁺ for MgS-1 samples (Table S5 in the Supporting Information). No signal attributable to the nano-sized MgO (a wide peak centered at about 26 ppm)^[55] is detected in the ²⁵Mg MAS NMR spectra for ²⁵MgS-1(30) (Figure 5), suggesting that rare MgO forms in the pores after calcination. In addition, expansion rather than shrinkage of the unit-cell parameters is observed after calcination of the MgS-1(30) sample (Figure S6 in the Supporting Information), not only revealing the stability

of the framework Mg species but also excluding the possibility formation of MgO in the pores. As shown in Scheme 2, the negatively charged oxygen atoms bonded to the framework Ae species contribute to the basicity of the AeS-1 samples.

Framework Ae ions of AeS-1 zeolites possess low electronegativity and are covalently bonded to the oxygen atoms in the MFI skeleton, which enables electron transfer from the metal ions to the oxygen atoms; thus, generating more negative oxygen



Scheme 2. Potential basic site in MgS-1 samples.

atoms that can be the origin of the strongly basic sites. Conversely, alkaline-earth metal oxide (AeO) impregnated analogues present weaker basicity with much inferior catalytic activity than the AeS-1 series, suggesting that the extra-framework Ae ions are unable to introduce the strongly basic sites. To confirm the above speculation, ¹H→¹³C and ¹H→²⁹Si CP MAS NMR studies of ethyl cyanoacetate (the substrate of the Knoevenagel condensation) adsorbed on the zeolites were carried out. For S-1 and MgS-1(30), similar ¹H→¹³C signals, but very different ¹H→²⁹Si CP signals were observed in the MAS NMR spectra of ethyl cyanoacetate (Figure 8).

Three resonances at -98, -102, and -114 ppm can be observed for MgS-1(30) in the ¹H→²⁹Si CP MAS NMR spectrum. The intensities of the former two peaks are comparable to each other but stronger than the latter one. It is not surprising to observe a strong signal for the peak at -98 ppm, which originates from Si close to H (Si-O-H groups). The resonance at -102 ppm, arising from Si-O-Mg, is enhanced significantly in CP with ethyl cyanoacetate, which results from the strong dipolar coupling effect between H in the adsorbed ethyl cyanoacetate and Si atoms in the Si-O-Mg environment. The results indicate that the framework Mg²⁺ site is indeed such a basic site that the acidic substrate tend to be adsorbed nearby. Otherwise, inert resonance should have been observed at -102 ppm. In contrast, the spectrum for ethyl cyanoacetate adsorbed over S-1 exhibits very small signals, implying very weak interactions because of the weak basicity of S-1. The above observations prove that the framework Mg species are responsible for the strongly basic sites.

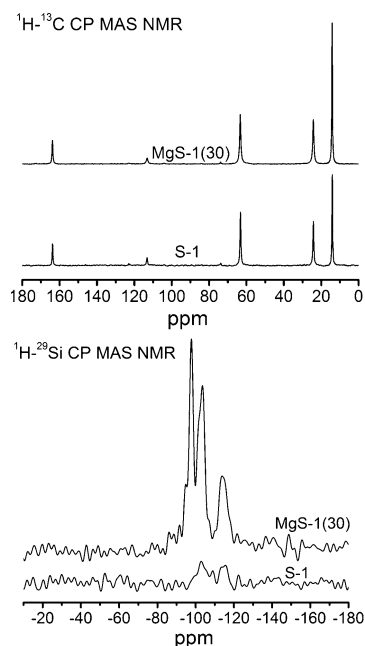


Figure 8. $^1\text{H}\rightarrow^{13}\text{C}$ and $^1\text{H}\rightarrow^{29}\text{Si}$ CP MAS NMR spectra of ethyl cyanoacetate adsorbed over S-1 and MgS-1(30).

Conclusion

Alkaline-earth metal-containing MFI-structured Al-free silicalite-1 zeolites, named as AeS-1 (Ae: alkaline-earth metal ions of Mg, Ca, Sr, and Ba; S-1: silicalite-1), were obtained through the one-pot hydrothermal approach involving the acidic co-hydrolysis/condensation of the silica source with Ae salts. Typical samples of MgS-1 exhibit apparent enlargement of unit-cell volume, additional IR vibrations at approximately $970\text{--}1000\text{ cm}^{-1}$, and new UV/Vis absorbance at approximately 245 nm, which are all absent for the parent pure S-1 and the impregnated analogue MgO/S-1, suggesting that variation of the pure silica MFI framework must have occurred through the introduction of Mg ions. Moreover, the unique ^{29}Si MAS NMR signal at -102 ppm for MgS-1, which is missing for S-1 and MgO/S-1, can be assigned to the framework Mg species by careful analysis of the ^{29}Si and $^1\text{H}\rightarrow^{29}\text{Si}$ CP MAS NMR spectra. The proposal is further supported by the ^{25}Mg NMR analysis for the ^{25}Mg isotope enriched $^{25}\text{MgS-1(30)}$ sample that was subjected to calcination, water adsorption, and re-calcination pretreatments. Therefore, though still short of direct evidence of the detailed exact structure of the Mg species in MgS-1 zeolites, the step-by-step comparative and complementary characterizations of this work allow us to propose the formation of framework Mg^{2+} species, alternatively, isolated Mg^{2+} species covalently bonded to the framework oxygen. This does not exclude the existence of extra-framework MgO species; indeed, these are detectable when the Mg loading is high in the MgS-1 series. Catalytic assessment indicates stable and higher activity over MgS-1 for the Knoevenagel condensation reaction than over the MgO-impregnated analogue and other control catalysts. Systematic base analyses demonstrate that MgS-1 exhibits strong basicity that stems from the framework Mg^{2+}

species, which are responsible for the better catalytic performance. This work provides the first family of strong solid base materials with well-defined microporous zeolitic structure, which could be potentially very important for heterogeneous base-catalyzed shape-selective reactions.

Experimental Section

Synthesis

All chemicals were of analytical grade and used as received. The typical synthesis procedure of MgS-1 was as follows: First, an aqueous solution of hydrochloric acid (12 M) was added into the aqueous solution of TEOS (10.0 g TEOS, 32.5 deionized water) under intense stirring at pH 1.0; this was followed by addition of a precalculated amount of magnesium nitrate hexahydrate. The resultant mixture was stirred at $20\text{ }^\circ\text{C}$ for 20 h to obtain complete co-hydrolysis of TEOS with the magnesium salt. TPABr (tetrapropylammonium bromide, 1.2 g) was then introduced into the mixture with stirring at room temperature. After that, aqueous NaOH solution (12.5 M) was added to induce the gelation at pH 5.0–6.0 and the mixture was stirred for 0.5 h. Finally, the pH value of the mixture was regulated to 10.0 by the careful addition of NaOH solution (12.5 M). After aging at room temperature for 10 h, the slurry was transferred to a Teflon-lined stainless steel autoclave and left to crystallize statically at $180\text{ }^\circ\text{C}$ for a preset time. Solid product was separated by centrifugation, washed with deionized water, and air-dried. The obtained as-synthesized samples were calcined at $550\text{ }^\circ\text{C}$ for 5 h in an air stream to obtain the final as-calcined solids. The products are designated MgS-1(*n*), where *n* stands for the Si/Mg molar ratio in the initial gel. Accordingly, CaS-1(*n*), SrS-1(*n*), and BaS-1(*n*) were synthesized by employing calcium nitrate tetrahydrate, strontium nitrate, and barium nitrate, respectively. Silicalite-1 was synthesized by similar procedures as above without adding alkaline-earth salts.

For comparison, the conventional method for the synthesis of heteroatomic zeolites was employed to synthesize the typical control samples for MgS-1(100), CaS-1(100), SrS-1(100), and BaS-1(100). TEOS and the corresponding alkaline-earth salts were co-hydrolyzed in basic media (using the aqueous solution of sodium hydroxide instead of hydrochloric acid), with the other procedures being the same as the above acidic co-hydrolysis route. The other control samples, AeO/S-1 (Ae = Mg, Ca, Sr, or Ba) were obtained by incipient wetness impregnation of alkaline-earth salts onto silicalite-1. A calculated amount $\text{Mg}(\text{NO}_3)_2\cdot 6\text{H}_2\text{O}$ (0.0804 g) was dissolved in water (1 mL) and then mixed with S-1 powder (1 g). After stirring for 2 h, the mixture was evaporated at $80\text{ }^\circ\text{C}$ to remove the majority of the water and then dried at $80\text{ }^\circ\text{C}$ for 24 h. After that, the solid product was calcined at $550\text{ }^\circ\text{C}$ for 5 h in an air stream, giving the final MgO/S-1 sample with the MgO loading amount of 1.87 wt%. In other words, the Si/Mg ratio of MgO/S-1 is same as MgS-1(30). Other AeO/S-1 (Ae = Ca, Sr, or Ba), with the Ae content the same as AeS-1(100), were prepared similarly. The ^{25}Mg isotopically labeled MgS-1(30) and MgO/S-1 were synthesized by using the ^{25}Mg isotopically labeled precursor $^{25}\text{Mg}(\text{NO}_3)_2$. Pure ZSM-5 in sodium form and ferric-containing heteroatomic ZSM-5 (named FeZSM-5(100)) were prepared according to ref. [33]. The commercial powder MgO (content $\geq 98\%$) was purchased from West Long Chemical Co., China. Highest impurity content: ignition loss (2.0%), carbonate (1.5%), hydrotrope (0.5%), sulfate (0.2%), sodium (0.05%), calcium (0.02%), chloride (0.01%). The nitrogen sorption results and XRD pattern of MgO are shown in Figures S7 and S8 in the Supporting Information.

Characterization

X-ray diffraction (XRD) patterns were collected on a SmartLab diffractometer (Rigaku Corporation) equipped with a rotating anode Cu source (9 kW) at 45 kV and 200 mA, from 5 to 50° with a scan rate of 2° min⁻¹. The morphology of the samples was tested with scanning electron microscopy (HITACHI S-4800). Energy-dispersive X-ray (EDX) analysis and elemental mapping were also obtained on this instrument with an acceleration voltage of 20 kV. Chemical compositions of samples were analyzed by using a Thermo Fisher iCAP 6300 inductively coupling plasma (ICP) spectrometer. BET surface areas were measured at the temperature of liquid nitrogen by using a Micromeritics ASAP2020 analyzer. Thermogravimetric (TG) analysis was carried out with a NETZSCH 449 F3 instrument in dry air at a heating rate of 10 °C min⁻¹. The FTIR spectra were obtained with a Nicolet 8700 FTIR spectrometer. Diffuse reflectance UV/Vis spectra were measured with the Shimadzu UV2600 spectrometer. CO₂ sorption experiments were conducted on a Micromeritics ASAP 2020m. The sample was pretreated at 573 K for 6 h in a He atmosphere, and maintained at 373 K during the sorption process.

The base strengths of the samples were measured by using a series of Hammett indicators, including 2,4-dinitroaniline (pK_a = 15.0), 4-nitroaniline (pK_a = 18.4), benzidine (pK_a = 22.5), 4-chloroaniline (pK_a = 26.5), and aniline (pK_a = 27.0).^[56] These indicators are listed in Table S6 in the Supporting Information, together with their colors. They were commercial reagents purified by recrystallization. Each indicator was dissolved in benzene for the preparation of a 0.5 wt% solution. The solid sample (100 mg) was pretreated at 600 °C for 2 h, and then transferred into benzene (2 mL) under a nitrogen atmosphere, followed with the addition of 2–3 drops of indicator solution. The color of the indicator adsorbed on the solid was observed visually. Solids with a base intensity (*H*₊) that exceeds the pK_a of the indicator will exhibit a color change.

Solid-state NMR experiments were performed on a Bruker Avance III spectrometer at an external magnetic field of 9.4 T with a 7 mm double-tuned MAS probe at a spinning rate of 6 kHz. ²⁹Si MAS NMR spectra were recorded with high-power ¹H decoupling using a short excitation pulse of π/8 (1.1 s) with a recycle delay of 10 s and with 5000 scans. ¹H → ²⁹Si cross polarization (CP) MAS NMR spectra were acquired with a contact time of 1 ms, recycle delay of 0.5 s, and 20 000 scans. ²⁹Si shifts were referenced to tetramethylsilane (TMS) at 0 ppm. ²⁵Mg MAS NMR spectra for zeolites were recorded using a rotor-synchronized Hahn-echo pulse sequence for spin-5/2 quadrupolar nuclei (π/6–τ–π/3–τ–acq.). A π/6 pulse length of 4.2 μs and a recycle delay of 0.1 s were used. ²⁵Mg solution NMR was used to monitor the environment of the Mg species during different stages of the co-hydrolysis step of MgS-1(30) as well as direct hydrolysis at pH 10.

NMR analysis of ¹³C-enriched CHCl₃ adsorbed on zeolites was performed as follows: A certain amount of ¹³C-enriched CHCl₃ (10 μmol g⁻¹ of CHCl₃ for each sample) was introduced to the dehydrated zeolite sample by a vacuum line before the sample was packed into a 7.0 mm rotor in a N₂ glovebox. ¹H → ¹³C CP MAS NMR experiments were performed with a contact time of 3 ms and a recycle delay of 4 s.

NMR analysis of ethyl cyanoacetate adsorbed on zeolites was carried out as follows: Ethyl cyanoacetate (0.1 mmol) and ethanol (5 mL) were mixed under a nitrogen atmosphere and heated to 70 °C; this was followed by addition of the catalyst (0.3 g) and stirring for 4 h. Then, the adsorbate-loaded catalyst was heated to 353 K under vacuum to remove ethanol. The sample was finally packed into a 7.0 mm rotor in a N₂ glovebox. ¹H → ¹³C CP MAS and ¹H → ²⁹Si CP MAS NMR measurements were performed with a con-

tact time of 4 ms and a recycle delay of 1 s. The chemical shifts of ¹H, ¹³C, and ²⁹Si were externally referenced to tetramethylsilane, and the chemical shift of ²⁵Mg was referenced to 0.1 M aqueous MgSO₄ solution, both of which were set at 0.0 ppm.

Catalytic assessment

The catalytic activity was assessed through the Knoevenagel condensation reaction by using different substrates, such as benzaldehyde and ethyl cyanoacetate. In a typical test, benzaldehyde (8 mmol), ethyl cyanoacetate (8 mmol), and ethanol (5 mL) were mixed under a nitrogen atmosphere and heated to 70 °C, followed by the addition of catalyst (0.1 g). The reaction slurry was stirred for 4 h under reflux conditions. After reaction, *n*-dodecane (0.85 g) was added as the internal standard. The reaction mixture was centrifuged and the liquid was analyzed by gas chromatography (Agilent GC 7890B equipped with a flame-ionization detector and a capillary column, HP-5; 30 m × 0.32 mm × 0.25 μm). In addition, a five-run recycling test was carried out. The catalyst was recovered by filtration, washed with ethanol, calcined at 550 °C, and then reused for the next run.

Acknowledgements

The authors greatly thank the National Natural Science Foundation of China (Nos. 21136005, 21303084, 21222302, and 21476109), the National Basic Research Program of China (No. 2013CB934800), the Jiangsu Province Science Foundation for Youths (No. BK20130921), the Specialized Research Fund for Doctoral Program of Higher Education (No. 20133221120002), and the Project of Priority Academic Program Development of Jiangsu Higher Education Institutions (PAPD).

Keywords: alkaline-earth metals · heterogeneous catalysis · hydrothermal synthesis · solid bases · zeolites

- [1] C. S. Cundy, P. A. Cox, *Chem. Rev.* **2003**, *103*, 663–701.
- [2] M. E. Davis, *Nature* **2002**, *417*, 813–821.
- [3] A. Primo, H. Garcia, *Chem. Soc. Rev.* **2014**, *43*, 7548–7561.
- [4] K. Na, C. Jo, J. Kim, K. Cho, J. Jung, Y. Seo, R. J. Messinger, B. F. Chmelka, R. Ryoo, *Science* **2011**, *333*, 328–332.
- [5] W. R. Gunther, Y. Wang, Y. Ji, V. K. Michaelis, S. T. Hunt, R. G. Griffin, Y. Román-Leshkov, *Nat. Commun.* **2012**, *3*, 1109.
- [6] A. Corma, *Chem. Rev.* **1995**, *95*, 559–614.
- [7] U. Olsbye, S. Svelle, M. Bjørgen, P. Beato, T. V. W. Janssens, F. Joensen, S. Bordiga, K. P. Lillerud, *Angew. Chem. Int. Ed.* **2012**, *51*, 5810–5831; *Angew. Chem.* **2012**, *124*, 5910–5933.
- [8] R. J. Davis, *J. Catal.* **2003**, *216*, 396–405.
- [9] G. J. Kramer, R. A. Santen, C. A. Emeis, A. K. Nowak, *Nature* **1993**, *363*, 529–531.
- [10] T. L. M. Maesen, R. Krishna, J. M. Baten, B. Smit, S. Calero, J. M. C. Sanchez, *J. Catal.* **2008**, *256*, 95–107.
- [11] H. Hattori, *Chem. Rev.* **1995**, *95*, 537–558.
- [12] F. Dogan, K. D. Hammond, G. A. Tompsett, H. Huo, W. C., Jr. Conner, S. M. Auerbach, C. P. Grey, *J. Am. Chem. Soc.* **2009**, *131*, 11062–11079.
- [13] T. C. Keller, S. Isabettoni, D. Verboekend, E. G. Rodrigues, J. Pérez-Ramírez, *Chem. Sci.* **2014**, *5*, 677–684.
- [14] X. F. Zhang, E. S. M. Lai, R. Martin-Aranda, K. L. Yeung, *Appl. Catal. A* **2004**, *261*, 109–118.
- [15] Y. Ono, *J. Catal.* **2003**, *216*, 406–415.
- [16] J. Weitkamp, M. Hunger, U. Ryma, *Microporous Mesoporous Mater.* **2001**, *48*, 255–270.
- [17] R. J. Davis, E. J. Dostkocil, S. Bordawekar, *Catal. Today* **2000**, *62*, 241–247.

- [18] M. J. Climent, A. Corma, S. Iborra, A. Velty, *J. Mol. Catal. A* **2002**, *182–183*, 327–342.
- [19] G. Busca, *Chem. Rev.* **2010**, *110*, 2217–2249.
- [20] D. Barthomeuf, *Catal. Rev. Sci. Eng.* **1996**, *38*, 521–612.
- [21] R. A. Schoonheydt, P. Geerlings, E. A. Pidko, R. A. Santen, *J. Mater. Chem.* **2012**, *22*, 18705–18717.
- [22] U. D. Joshia, P. N. Joshib, S. S. Tamhankarb, V. V. Joshic, C. V. Rodeb, V. P. Shiralkarb, *Appl. Catal. A* **2003**, *239*, 209–220.
- [23] L. Martins, W. Hölderich, D. Cardoso, *J. Catal.* **2008**, *258*, 14–24.
- [24] P. E. Hathaway, M. E. Davis, *J. Catal.* **1989**, *116*, 263–279.
- [25] M. D. Romero, G. Ovejero, A. Rodríguez, J. M. Gómez, I. Águeda, *Ind. Eng. Chem. Res.* **2004**, *43*, 8194–8199.
- [26] H. K. Min, S. H. Cha, S. B. Hong, *Chem. Commun.* **2013**, *49*, 1115–1117.
- [27] M. Hartmann, L. Kevan, *Chem. Rev.* **1999**, *99*, 635–663.
- [28] Y. T. Meng, H. C. Genuino, C. H. Kuo, H. Huang, S. Y. Chen, L. C. Zhang, A. Rossi, S. L. Suib, *J. Am. Chem. Soc.* **2013**, *135*, 8594–8605.
- [29] Y. J. Wu, J. Wang, P. Liu, W. Zhang, J. Gu, X. J. Wang, *J. Am. Chem. Soc.* **2010**, *132*, 17989–17991.
- [30] W. B. Fan, R. G. Duan, T. Yokoi, P. Wu, Y. Kubota, T. Tatsumi, *J. Am. Chem. Soc.* **2008**, *130*, 10150–10164.
- [31] Y. K. Hwang, J. S. Chang, S. E. Park, D. S. Kim, Y. U. Kwon, S. H. Jung, J. S. Hwang, M. S. Park, *Angew. Chem. Int. Ed.* **2005**, *44*, 556–560; *Angew. Chem.* **2005**, *117*, 562–566.
- [32] A. Corma, L. T. Nemeth, M. Renz, S. Valencia, *Nature* **2001**, *412*, 423–425.
- [33] J. Gu, Y. H. Jin, Y. Zhou, M. J. Zhang, Y. J. Wu, J. Wang, *J. Mater. Chem. A* **2013**, *1*, 2453–2460.
- [34] A. Corma, R. M. Martín-Aranda, F. Sánchez, *J. Catal.* **1990**, *126*, 192–198.
- [35] S. H. Park, H. Liu, M. Kleinsorge, C. P. Grey, B. H. Toby, J. B. Parise, *Chem. Mater.* **2004**, *16*, 2605–2614.
- [36] B. Q. Xu, J. M. Wei, H. Y. Wang, K. Q. Sun, Q. M. Zhu, *Catal. Today* **2001**, *68*, 217–225.
- [37] S. K. Saha, S. B. Waghmode, H. Maekawa, K. Komura, Y. Kubota, Y. Sugii, Y. Oumi, T. Sano, *Microporous Mesoporous Mater.* **2005**, *81*, 289–303.
- [38] L. Wang, Y. P. Xu, B. C. Wang, S. J. Wang, J. Y. Yu, Z. J. Tian, L. W. Lin, *Chem. Eur. J.* **2008**, *14*, 10551–10555.
- [39] N. Maxim, P. C. M. M. Magusin, P. J. Kooyman, J. H. M. C. van Wolput, R. A. van Santen, H. C. L. Abbenhuis, *Chem. Mater.* **2001**, *13*, 2958–2964.
- [40] J. M. Garces, US Patent 4,732,747, **1988**.
- [41] E. M. Flanigen, J. M. Bennett, R. W. Grose, J. P. Cohen, R. L. Patton, R. M. Kirschner, J. V. Smith, *Nature* **1978**, *271*, 512–516.
- [42] N. Hedin, G. J. DeMartin, W. J. Roth, K. G. Strohmaier, S. C. Reyes, *Microporous Mesoporous Mater.* **2008**, *109*, 327–334.
- [43] H. P. Lin, C. Y. Mou, *Acc. Chem. Res.* **2002**, *35*, 927–935.
- [44] K. J. D. MacKenzie, M. E. Smith, *Multinuclear Solid-State Nuclear Magnetic Resonance*, Ch. 4, Elsevier, Oxford, **2002**.
- [45] C. A. Fyfe, Y. Feng, H. Grondey, G. T. Kokotailo, H. Gies, *Chem. Rev.* **1991**, *91*, 1525–1543.
- [46] C. A. Fyfe, H. Grondey, Y. Feng, G. T. Kokotailo, *J. Am. Chem. Soc.* **1990**, *112*, 8812–8820.
- [47] H. Morell, K. Angermund, A. R. Lewis, D. H. Brouwer, C. A. Fyfe, H. Gies, *Chem. Mater.* **2002**, *14*, 2192–2198.
- [48] J. A. van Bokhoven, D. C. Koningsberger, P. Kunkeler, H. Bekkum, A. P. M. Kentgens, *J. Am. Chem. Soc.* **2000**, *122*, 12842–12847.
- [49] J. Jiao, S. Altwasser, W. Wang, J. Weitkamp, M. Hunger, *J. Phys. Chem. B* **2004**, *108*, 14305–14310.
- [50] M. Sánchez-Sánchez, T. Blasco, F. Rey, *Phys. Chem. Chem. Phys.* **1999**, *1*, 4529–4535.
- [51] X. B. Wang, X. F. Zhang, Y. Wang, H. O. Liu, J. S. Qiu, J. Q. Wang, W. Han, K. L. Yeung, *ACS Catal.* **2011**, *1*, 437–445.
- [52] E. Angelescu, O. D. Pavel, R. Birjega, R. Zavoianu, G. Costentin, M. Che, *Appl. Catal. A* **2006**, *308*, 13–18.
- [53] M. Boronat, M. J. Climent, A. Corma, S. Iborra, R. Montón, M. Sabater, *Chem. Eur. J.* **2010**, *16*, 1221–1231.
- [54] K. Sugahara, T. Kimura, K. Kamata, K. Yamaguchi, N. Mizuno, *Chem. Commun.* **2012**, *48*, 8422–8424.
- [55] A. V. Chadwick, I. J. F. Poplett, D. T. S. Maitland, M. E. Smith, *Chem. Mater.* **1998**, *10*, 864–870.
- [56] J. I. Take, N. Kikuchi, Y. Yoneda, *J. Catal.* **1971**, *21*, 164–170.

Received: May 14, 2015

Published online on September 2, 2015